INTERNATIONAL JOURNAL FOR NUMERICAL METHODS IN ENGINEERING, VOL. 24, 1721–1739 (1987)

NOTES ON THE STABILITY OF NON-RECTANGULAR SPACE–TIME FINITE ELEMENTS

CZESŁAW I. BAJER†

Institut National Polytechnique de Lorraine, LA.R.A.M.A.O., Parc de Saurupt, 54042 NANCY Cedex, France

SUMMARY

The method of space–time finite elements enables the simple solution of quite new problems. It is possible to assume the arbitrary partition of the structure area in each moment of integration of the motion equation. Instability is caused by a too large time step and too great changes of joint locations in successive time steps. A changeable spatial partition is useful in contact dynamic problems, in the case of a travelling support, generally in problems with movable edges. In this paper a stability problem is described and some investigations for chosen types of non-rectangular space–time finite elements are carried out. Linear and surface elements which in time space gain an additional time dimension are presented. Some numerical examples prove the efficiency of the described method under determined limitations.

INTRODUCTION

In static analysis of structures, a division of an object into finite elements is always carried out along some characteristic curves, for example in places where thickness or material properties are changed. Point forces are often located in joints, and joints of the mesh are placed in points of support locations. The same rules should be taken into consideration in dynamic analysis. To provide the coincidence of the partition of a structure with characteristic curves in each moment, non-stationary division of the structure should be assumed. Lines limiting the plastic regions or the contact area of a beam or a plate placed on a unilateral foundation are good examples of the curves which are to be in coincidence with the element edges. Moreover, non-stationary joint location enables the solution of structures with movable boundary conditions, changeable geometry, etc. Some achievements in the solution of parabolic problems with a free boundary were described by Bonnerot and Jamet.[1,2]

There is another problem in non-linear vibration analysis of structures. The integration of the motion equation is often carried out with the same time step for the whole construction. The time step can be changed after several steps, but for the whole construction, not just for a portion. It is difficult to integrate a motion equation with a small time step only in regions of greater stiffness and high speed of deformations. Some aspects of this problem have been described in References 3 and 4. The mixed explicit–implicit scheme of integration enables the application of different time steps to different regions. The time step in the implicit portion is an integral multiple of the explicit time step, but the formulation of the solution scheme in multi-dimensional problems is complicated.

† Permanent address: Department of Civil Engineering, Engineering College of Zielona Góra, Podgórna 50, 65-246 Zielona Góra, Poland

0029–5981/87/091721–19$09.50

Received 18 February 1986
Revised 15 September 1986

The stationary division of the structure and the difficulties with the changeable time step are serious restrictions in commonly known methods of vibration analysis. The method enables non-stationary division of the structure and time partition condensation in some regions.[5] The space–time finite element approach was first described in References 6 and 7. The Hamilton principle was directly applied to the differential equation of motion. Further developments were published in References 8–12. A space–time finite element is a finite element in which an additional time dimension is considered. A uni-dimensional beam element has a two-dimensional shape in time and space and a space–time plate element has three dimensions. In first formulations of the space–time finite element method applied to vibration analysis, the rectangular division of the time space was assumed and the method was a conditionally stable one with regard to the time step. In the further elaborations the unconditional stability for rectangluar division of the time space was proved[13] and non-rectangular space–time elements were introduced.[5] But the only restriction which limits the simple use of the non-rectangular space–time elements is the stability problem. Experiments indicate that in applications of non-rectangular elements their shape is dictated by the stability restrictions and not by the accuracy requirements. Several papers were published on the stability and accuracy of integration methods.[14–20] However, they concern the stationary structure partition.

There are two reasons for instability of the solution schemes. The value of the time step in the integration of the motion equation is the first one. The time step is understood here as a time dimension of the space–time finite element. In non-linear problems the time step should be small enough to ensure that the model is sufficiently close to the real problem. In the case of non-rectangular elements it is difficult to express the influence of the time step on the stability. The influence of the geometry of the space–time elements is also difficult to show. It can be simply proved that the use of triangular, tetrahedral and hyper-tetrahedral elements (generally called simplex-shaped elements) is conducive to the system of algebraic equations with a triangular matrix of coefficients.[21,22] It can simplify the computations, allows the efficient use of the memory and enables the application of the method to small computers. This is why simplex-shaped elements are of special interest in the present analysis.

OUTLINE OF THE SPACE–TIME FINITE ELEMENT METHOD

For a better understanding of the hypotheses of this paper, a short introduction to the space–time finite element theory seems to be helpful. It was noted above that space–time elements have an additional time dimension. In Figure 1 examples of space–time elements are depicted. Only two main groups are presented: multiplex type (Figure 1(a)) and simplex type (Figure 1(b)). Many other shapes are available since the time space can be divided into subareas of any shape.

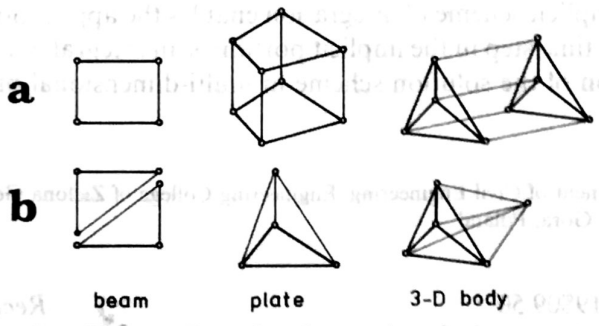

Figure 1. Examples of space–time elements

Displacements $\boldsymbol{\delta}_e(x, y, z, t)$ should be determined in all nodes of the space–time finite element (STFE). Inside the displacement vector $\mathbf{f}(x, y, z, t)$ is obtained by interpolation:

$$\mathbf{f} = \mathbf{N}\boldsymbol{\delta}_e \tag{1}$$

$\mathbf{N}$ is the matrix of shape functions. The stress vector $\boldsymbol{\sigma}(x, y, z, t)$ and strain vector $\boldsymbol{\varepsilon}(x, y, z, t)$ can be expressed by the commonly known relations

$$\boldsymbol{\sigma} = \left(\mathbf{E} + \eta_w \frac{\partial}{\partial t}\right)\boldsymbol{\varepsilon} \tag{2}$$

$$\boldsymbol{\varepsilon} = \partial_x \mathbf{f} = \partial_x \mathbf{N}\boldsymbol{\delta}_e \tag{3}$$

$\partial_x(x, y, z, t)$ is the matrix of differential operators, $\mathbf{E}$ is the elasticity constant matrix and η_w is a coefficient of internal damping (in the Kelvin–Voigt model). Deformations of the element in time (derivative of the displacement in terms of time) $\boldsymbol{\varepsilon}(x, y, z, t)$ can be determined as a velocity:

$$\boldsymbol{\varepsilon}_t = \frac{\partial \mathbf{f}}{\partial t} = \frac{\partial \mathbf{N}}{\partial t}\boldsymbol{\delta}_e \tag{4}$$

The negative momentum of the material point $\boldsymbol{\sigma}_t(x, y, z, t)$ equals

$$\boldsymbol{\sigma}_t = -\mathbf{R}\boldsymbol{\varepsilon}_t \tag{5}$$

$\mathbf{R}$ denotes the matrix of the elementary inertia coefficients. Denoting η_Z as an external damping coefficient, the virtual four-work (time-work, work integrated over time interval) of internal forces in the volume of the element can be equated to the four-work of external forces

$$\int_V (\delta\boldsymbol{\varepsilon}^{\mathrm{T}}\boldsymbol{\sigma} + \delta\boldsymbol{\varepsilon}_t^{\mathrm{T}}\boldsymbol{\sigma}_t)\,\mathrm{d}V = \delta\boldsymbol{\delta}_e^{\mathrm{T}}\mathbf{F}_e - \int_V \delta\mathbf{f}^{\mathrm{T}}\eta_Z \frac{\partial \mathbf{f}}{\partial t}\mathrm{d}V \tag{6}$$

The integration extends over the volume of the STFE $\mathbf{F}_e$ is a vector of nodal impulses. Considering (2), (3), (4) and (5) it can be written

$$\int_V \left[(\partial_x \mathbf{N})^{\mathrm{T}}\mathbf{E}\partial_x \mathbf{N} + (\partial_x \mathbf{N})^{\mathrm{T}}\eta_w \frac{\partial}{\partial t}\partial_x \mathbf{N} - \left(\frac{\partial}{\partial t}\mathbf{N}\right)^{\mathrm{T}}\mathbf{R}\frac{\partial}{\partial t}\mathbf{N} + \mathbf{N}^{\mathrm{T}}\eta_Z \frac{\partial}{\partial t}\mathbf{N}\right]\mathrm{d}V\,\boldsymbol{\delta}_e = \mathbf{F}_e \tag{7}$$

We notice that the same results can be obtained with the use of Galerkin's method applied to the differential equation with a time variable. Equation (7) can be extended over the whole structure. Then it can be written (sums are omitted)

$$(\mathbf{K} + \mathbf{M} + \mathbf{W} + \mathbf{Z})\boldsymbol{\delta} = \mathbf{F} \quad \text{or} \quad \hat{\mathbf{K}}\boldsymbol{\delta} = \mathbf{F} \tag{8}$$

where

$$\begin{aligned}
\mathbf{K} &= \int_V (\partial_x \mathbf{N})^{\mathrm{T}}\mathbf{E}\partial_x \mathbf{N}\,\mathrm{d}V \\
\mathbf{M} &= -\int_V \left(\frac{\partial}{\partial t}\mathbf{N}\right)^{\mathrm{T}}\mathbf{R}\frac{\partial}{\partial t}\mathbf{N}\,\mathrm{d}V \\
\mathbf{W} &= \int_V (\partial_x \mathbf{N})^{\mathrm{T}}\eta_w \frac{\partial}{\partial t}\partial_x \mathbf{N}\,\mathrm{d}V \\
\mathbf{Z} &= \int_V \mathbf{N}^{\mathrm{T}}\eta_Z \frac{\partial}{\partial t}\mathbf{N}\,\mathrm{d}V
\end{aligned} \tag{9}$$

Matrices **K**, **M**, **W** and **Z** are called stiffness, mass, internal damping and external damping matrices respectively. The analysis of the joint connection in several successive time layers leads to the infinite global matrix **K** in the form

$$\begin{bmatrix} \mathbf{A}_1 & \mathbf{B}_1 & & \\ \mathbf{C}_1 & \mathbf{D}_1+\mathbf{A}_2 & \mathbf{B}_2 & \\ & \mathbf{C}_2 & \mathbf{D}_2+\mathbf{A}_3 & \cdots \end{bmatrix} \begin{Bmatrix} \boldsymbol{\delta}_1 \\ \boldsymbol{\delta}_2 \\ \boldsymbol{\delta}_3 \\ \vdots \end{Bmatrix} = \begin{Bmatrix} \mathbf{F}_1 \\ \mathbf{F}_2 \\ \mathbf{F}_3 \\ \vdots \end{Bmatrix} \tag{10}$$

$\mathbf{A}_i, \mathbf{B}_i, \mathbf{C}_i$ and $\mathbf{D}_i$ are square submatrices of the matrix **K** evaluated for one space–time layer. The order of each of them is equal to the total number of degrees of freedom in the structure. Such a formulation enables step-by-step solution:

$$\boldsymbol{\delta}_{i+1} = \mathbf{B}_i^{-1}\mathbf{F}_i - \mathbf{B}_i^{-1}(\mathbf{D}_{i-1}+\mathbf{A}_i)\boldsymbol{\delta}_i - \mathbf{B}_i^{-1}\mathbf{C}_{i-1}\boldsymbol{\delta}_{i-1} \tag{11}$$

In this meaning the space–time finite element method can be regarded as an explicit time integration method. However, the time space can be divided into elements of almost any shape.

STABILITY ANALYSIS

General formulation

In the investigation of the solution schemes approximated by a non-rectangular mesh, it is noted that in some cases unstable solutions are obtained. To examine the stability problem the system of elements shown in Figure 2 was used. The simplest mesh has been chosen to investigate the influence of only the parameter d on the stability criterion. The selection of the type of mesh geometry allows us to treat the worst case. In any other, even more complicated system with a non-stationary joint location we can expect milder restrictions. Each second layer of nodes was eliminated and in this way reproducible superelements were obtained. The matrix of the system of equations can be written in a block form

$$\begin{bmatrix} \mathbf{F} & \mathbf{A} & \mathbf{B} & & (0) \\ & \mathbf{C} & \mathbf{D} & \mathbf{E} & \\ & & \mathbf{F} & \mathbf{A} & \mathbf{B} \\ (0) & & & \mathbf{C} & \mathbf{D} & \mathbf{E} \\ & & & & \ddots & \ddots & \ddots \end{bmatrix}$$

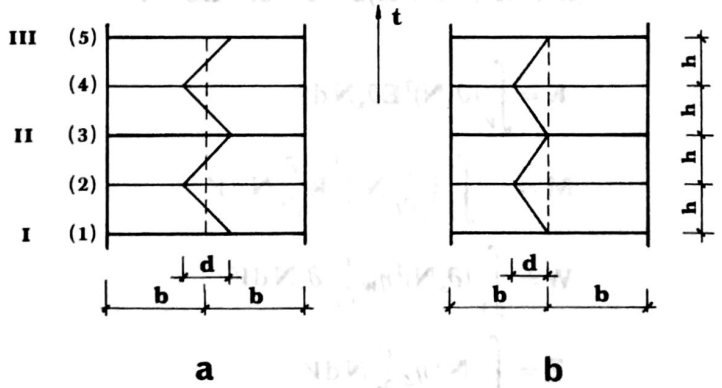

Figure 2. A part of the analysed space–time band

For free vibrations an equation of the step-by-step process is obtained (see Reference 5):

$$(-\mathbf{F}\mathbf{D}^{-1}\mathbf{C})\boldsymbol{\delta}_{\mathrm{I}}+(\mathbf{A}-\mathbf{F}\mathbf{D}^{-1}\mathbf{E}-\mathbf{B}\mathbf{D}^{-1}\mathbf{C})\boldsymbol{\delta}_{\mathrm{II}}+(-\mathbf{B}\mathbf{D}^{-1}\mathbf{E})\boldsymbol{\delta}_{\mathrm{III}}=\mathbf{0} \tag{12}$$

The same can be written with the use of transfer matrix $\mathbf{T}$:

$$\begin{Bmatrix}\boldsymbol{\delta}_{i+1}\\ \boldsymbol{\delta}_i\end{Bmatrix}=\mathbf{T}\begin{Bmatrix}\boldsymbol{\delta}_i\\ \boldsymbol{\delta}_{i-1}\end{Bmatrix} \tag{13}$$

where

$$\mathbf{T}=\begin{bmatrix}(\mathbf{B}\mathbf{D}^{-1}\mathbf{E})^{-1}(\mathbf{A}-\mathbf{F}\mathbf{D}^{-1}\mathbf{E}-\mathbf{B}\mathbf{D}^{-1}\mathbf{C}) & -(\mathbf{B}\mathbf{D}^{-1}\mathbf{E})^{-1}\mathbf{F}\mathbf{D}^{-1}\mathbf{C}\\ \mathbf{I} & \mathbf{0}\end{bmatrix} \tag{14}$$

The stability condition for the problem (13) was described in References 23 and 24. If the spectral radius ψ of the matrix $\mathbf{T}$ is less than or equal to one the solution scheme (12) is stable:

$$\psi(\mathbf{T})\leqslant 1 \tag{15}$$

In the case of $\psi(\mathbf{T})=1$ when the spectral radius is a multiple root of the characteristic equation the problem (12) is also unstable. Matrix $\mathbf{T}$ can be regarded as an amplification matrix of vibrations. Because of the symmetry of the space–time stiffness matrix $\mathbf{K}$, we can reduce the right-hand upper submatrix of $\mathbf{T}$ (equation (14)) to the minus identity matrix. Then the condition

$$\det(\mathbf{T}-\lambda\mathbf{I})=0,\quad |\lambda_i|\leqslant 1 \tag{16}$$

in the case of one degree of freedom can be reduced to the relation:

$$|T_{11}|\leqslant 2 \tag{17}$$

Stability of longitudinal vibrations of prismatic rods

In cases of simple structures the stability analysis can be carried out analytically. A bar element in axial vibration has one degree of freedom in each node and due to this it is a good object for our investigation. The system of the space–time elements shown in Figure 2 consists of four trapezoidal elements. If the nodes on the edges are fixed, the global stiffness and mass coefficients can be simply derived.

Let us assume a linear transformation of the trapezoidal into a square:

$$x=\sum_{i=1}^{4}\bar{N}_i x_i\quad t=\sum_{i=1}^{4}\bar{N}_i t_i \tag{18}$$

where

$$\bar{N}_i(\xi,\tau)=\tfrac{1}{4}(1+\xi\xi_i)(1+\tau\tau_i) \tag{19}$$

and x_i, t_i are nodal co-ordinates in the global co-ordinate system and ξ_i, τ_i nodal co-ordinates in the local co-ordinate system.

The axial displacement is the only unknown displacement in the bar element. The displacement f in any point of the element is expressed in terms of the nodal values $\boldsymbol{\delta}$

$$f=\sum_{i=1}^{4}N_i(\xi,\tau)\boldsymbol{\delta}_i=\mathbf{N}\boldsymbol{\delta} \tag{20}$$

The shape functions $\mathbf{N}_i(\xi,\tau)$ are determined as simple linear relations described as in (19). The strain and stress are expressed by the relations

$$\varepsilon=\frac{\partial f}{\partial x}=\frac{\partial \mathbf{N}}{\partial x}\boldsymbol{\delta} \tag{21}$$

$$\sigma = EA\varepsilon = EA\frac{\partial f}{\partial x} \tag{22}$$

where EA is the axial stiffness coefficient.

Deformations of the element in time ε_t can be determined as a velocity

$$\varepsilon_t = \frac{\partial f}{\partial t} = \frac{\partial \mathbf{N}}{\partial t}\boldsymbol{\delta} \tag{23}$$

The momentum of the material point σ_t (with the mass density ρ) is

$$\sigma_t = -\rho A\varepsilon_t \tag{24}$$

It was shown for example in References 9 and 11 that the stiffness **K** and mass **M** matrix coefficients are given by the integrals

$$\mathbf{K} = \int_V \left(\frac{\partial \mathbf{N}}{\partial x}\right)^{\mathrm{T}} EA\frac{\partial \mathbf{N}}{\partial x}\,\mathrm{d}V \tag{25}$$

$$\mathbf{M} = -\int_V \left(\frac{\partial \mathbf{N}}{\partial t}\right)^{\mathrm{T}} \rho A\frac{\partial \mathbf{N}}{\partial t}\,\mathrm{d}V \tag{26}$$

and the matrix equation of motion is of the form

$$(\mathbf{K}+\mathbf{M})\boldsymbol{\delta} = \mathbf{Q} \quad \text{or} \quad \hat{\mathbf{K}}\boldsymbol{\delta} = \mathbf{Q} \tag{27}$$

Q is the vector of nodal impulses.

The coefficients of **A**, **B**, ..., **F** in (14) for the mesh with fixed edges (Figure 2(a)) were evaluated:

$$\mathbf{A} = \left(\frac{EAh}{d^3} - \frac{\rho A}{3hd}\right)(d^2+4b^2)\ln\frac{2b+d}{2b-d} - \frac{4EAhb}{d^2} \tag{28}$$

$$\mathbf{B} = \left(\frac{EAh}{2d^3} - \frac{\rho A}{6hd}\right)(d^2-4b^2)\ln\frac{2b+d}{2b-d} + \frac{2EAhb}{d^2} \tag{29}$$

$$\mathbf{C} = \mathbf{E} = \mathbf{F} = \mathbf{B}, \quad \mathbf{D} = \mathbf{A} \tag{30}$$

Now the amplification matrix **T** can be reduced to the simple form

$$\mathbf{T} = \begin{bmatrix} \left(\dfrac{\mathbf{A}}{\mathbf{B}}\right)^2 - 2 & -1 \\ 1 & 0 \end{bmatrix} \tag{31}$$

The spectral radius of (31) is equal to 1 when the roots of the characteristic polynomial of **T** are complex. Let us introduce dimensionless parameters

$$s = \frac{d}{h}\frac{1}{c}, \quad c^2 = E/\rho \tag{32}$$

$$k = \frac{d}{b}, \quad 0 \leqslant k \leqslant 2 \tag{33}$$

The stability area can be determined in terms of k and s. It is bounded by the curves

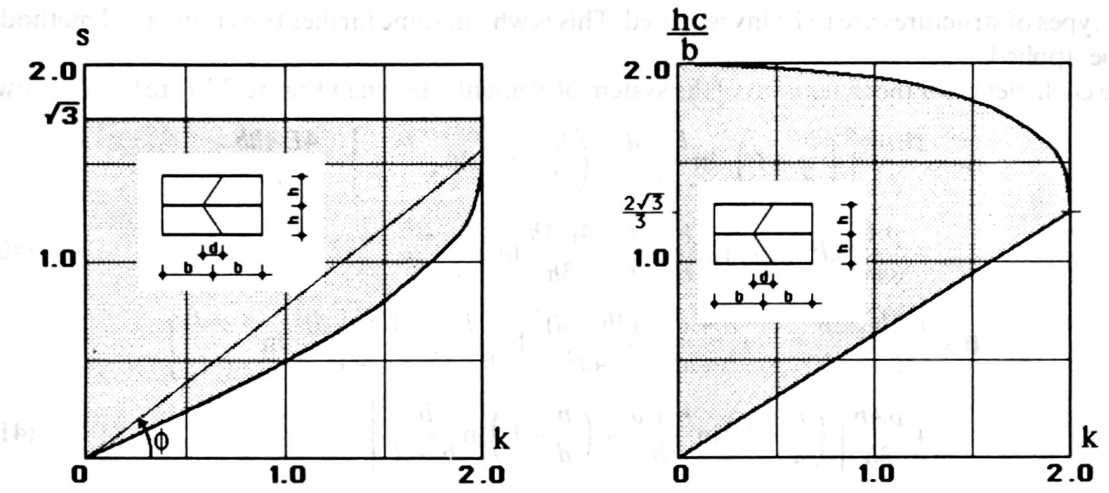

Figure 3. Area of stability for the axial vibrations of bars (quadrangular elements) in two alternative systems of co-ordinates

$$\left(3-\frac{3k}{\ln\dfrac{2+k}{2-k}}\right)^{1/2}\leqslant s\leqslant\sqrt{3} \tag{34}$$

Inequalities (34) are depicted in Figure 3. The tangent of the slope of any straight line carried through the origin of the co-ordinates is defined by the value that is the inversion of the Courant number:

$$\mathrm{tg}\phi=\frac{b}{ch} \tag{35}$$

Each straight line determines the stability points of the problem in which h is the only variable. It can be noticed that the full stability range of k is obtained only on the line for which

$$\mathrm{tg}\phi=\frac{\sqrt{3}}{2} \tag{36}$$

It occurs when the time step h equals

$$h=\frac{2}{\sqrt{3}}\frac{b}{c} \tag{37}$$

The critical time step h_{cr} can be evaluated by the consideration of (34) and (35):

$$\left.\frac{\mathrm{d}s}{\mathrm{d}k}\right|_{k=0}=\frac{1}{2} \tag{38}$$

and it reduces to the condition

$$h\leqslant\frac{2b}{c} \tag{39}$$

In addition, we can recall that in the case of a stationary joint location the central difference method is restricted by the condition $h\leqslant\sqrt{2}\,b/c$.

Analytical calculations in the case shown in Figure 2(b) are complicated. The same occurs when

other types of structures are to be investigated. This is why in some further tests numerical methods will be applied.

The coefficients for the inner joint of the system of elements shown in Figure 2(b) are listed below:

$$\mathbf{A} = \frac{2EAh}{d}\left[\left(\frac{b}{d}+1\right)^2 \ln\frac{b+d}{b} + \left(\frac{b}{d}-1\right)^2 \ln\frac{b}{b-d}\right] - \frac{4EAhb}{d^2} - \frac{\rho A}{6hd}(3d^2+4b^2)\ln\frac{b+d}{b-d} - \frac{4\rho Ab}{3h}\ln\frac{b^2-d^2}{b^2} \tag{40}$$

$$\mathbf{B} = \frac{EAh}{d}\left[\frac{2b}{d} + \frac{1}{4}\ln\frac{b+d}{b-d} - \frac{(2b-d)^2}{4d^2}\ln\frac{b}{b-d} - \frac{(2b+d)^2}{4d^2}\ln\frac{b+d}{b}\right] + \frac{\rho Ab}{3h}\left[\left(\frac{b}{d}+1\right)\ln\frac{b+d}{b} + \left(\frac{b}{d}-1\right)\ln\frac{b}{b-d}\right] \tag{41}$$

$$\mathbf{D} = \frac{2EAhb^2}{d^3}\ln\frac{b+d}{b-d} - \frac{4EAhb}{d^2} - \frac{2\rho Ab^2}{3hd}\ln\frac{b+d}{b-d} \tag{42}$$

$$\mathbf{C} = \mathbf{E} = \mathbf{F} = \mathbf{B} \tag{43}$$

The stability diagram for this case is plotted in Figure 4. It is similar to the one presented in Figure 3, although the horizontal co-ordinate $k' = d/b$ is related to the initial length of a spatial element. Then only half of the width of the diagram can be interpreted. For $k' > 1$ the system of elements is degenerated. If we mark the ratio of the value d related to the average length of the element according to the relation

$$k = \frac{d}{b-\frac{d}{2}} = \frac{2k'}{2-k'} \quad 0 \leqslant k' \leqslant 1, \quad 0 \leqslant k \leqslant 2 \tag{44}$$

we can plot the stability region in terms of the same parameter k as in Figure 3. The lower part of the diagram is undoubtedly caused by the longer right-hand element for which the average spatial length is equal to $b + d/2$.

The properties of quadrangular element stability can be explained extensively after consider-

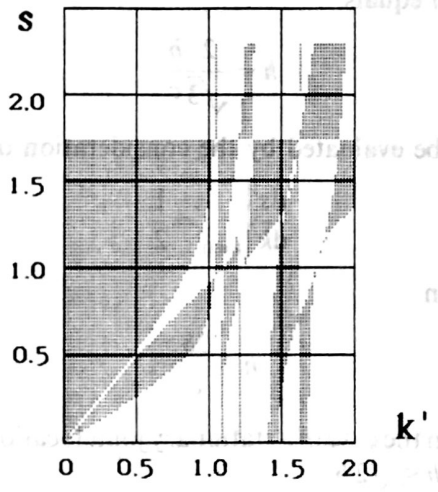

Figure 4. Stability area for the bar elements with the mesh from Figure 2(b)

ation of the system of triangular elements of a bar in axial vibration. Alternate space–time elements have oppositely directed slope edges. The assumption of a linear time and space distribution of displacements gives the values of coefficients

$$\mathbf{A} = \frac{32EAhb}{4b^2 - d^2} - \frac{4\rho A(4b^2 + d^2)}{h(2b + d)}, \quad \mathbf{D} = \mathbf{A} \tag{45}$$

$$\mathbf{B} = \frac{2\rho A(2b - d)}{h}, \qquad \mathbf{C} = \mathbf{E} = \mathbf{F} = \mathbf{B} \tag{46}$$

The eigenvalue problem of (14) leads to the inequalities

$$(1) \quad -2 \leqslant k \leqslant 0 \qquad s > \sqrt{\left(\frac{8}{2-k}\frac{k^2}{4+k^2}\right)} \tag{47}$$

$$(2) \quad 0 \leqslant k \leqslant 2 \qquad s > \frac{k}{\sqrt{(2-k)}} \tag{48}$$

$$(3) \quad -2 \leqslant k \leqslant 2 \qquad s < \frac{2}{\sqrt{(2-k)}} \tag{49}$$

The diagram of relations (47)–(49) is shown in Figure 5. It can be seen that for $h < 0{\cdot}54\, b/c$ the interval of the stability cannot be simply connected. The condition (2) (equation (48)) describes the time step h for the stationary mesh (then $k = 0$)

$$\left.\frac{ds}{dk}\right|_{k=0} = \frac{\sqrt{2}}{2} \tag{50}$$

Considering (35), we can obtain the critical value

$$h_{cr} = \sqrt{2}\frac{b}{c} \tag{51}$$

The identical condition is obtained for the central difference method. It is worth emphasizing that, if triangular elements are used in the mesh with a stationary joint location, the recurrence formula obtained by the triangular space–time finite elements is identical with the one obtained by the

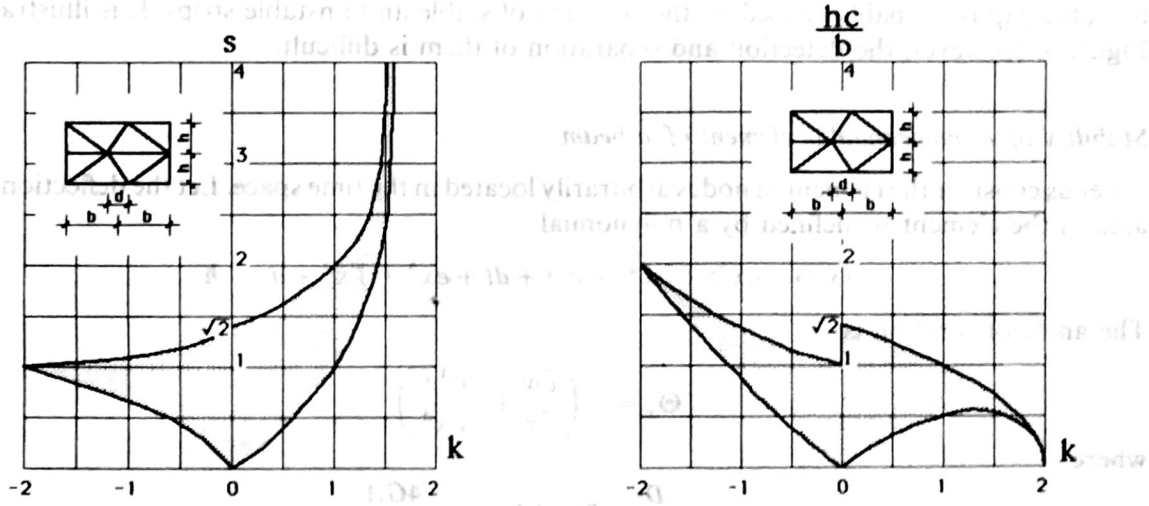

Figure 5. Area of stability for the triangular elements of a bar in two alternative systems of co-ordinates

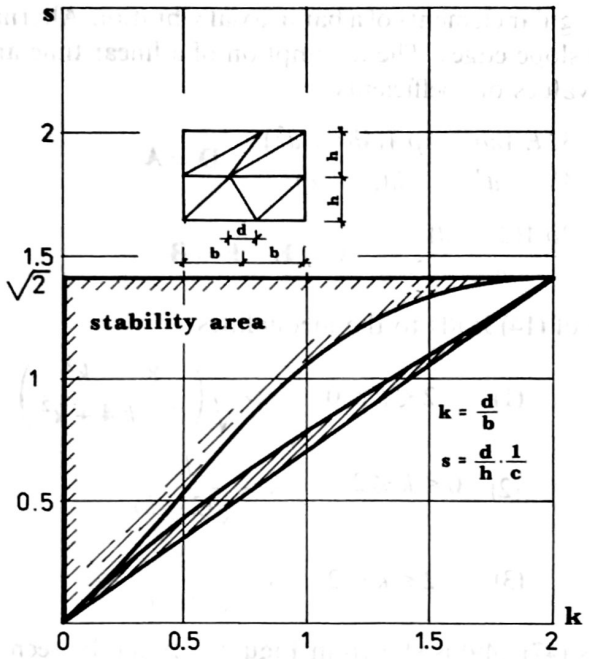

Figure 6. Area of stability for the triangular elements of a bar (regular mesh)

central difference method. The way that the space–time layer is divided into space–time elements has no influence in this case.

When the space–time layers are reproducible (considering the sense of slope edges) the result of numerical searching of the stability area is depicted in Figure 6. The stable region is bounded by the inequality

$$\frac{\sqrt{2}}{2}k \leqslant s \leqslant \sqrt{2}, \qquad 0 \leqslant k \leqslant 2 \tag{52}$$

However, the region of stability is not simply connected. Even small viscous damping does not remove the instability inside the stable region. Moreover, the viscous damping does not change the critical time step (Figure 7), although the upper limit for the parameter s slightly increases. The unstable gap is probably caused by the covering of stable and unstable strips. It is illustrated in Figure 4. However, the detection and separation of them is difficult.

Stability of a quadrangular element of a beam

Let us consider the element of nodes arbitrarily located in the time space. Let the deflection in the area of the element be defined by a polynomial:

$$w(x,t) = ax^3t + bx^2t + cxt + dt + ex^3 + fx^2 + gx + h \tag{53}$$

The angle of rotation is

$$\Theta_x = -\left(\frac{\partial w}{\partial x} + \gamma\frac{\partial^3 w}{\partial x^3}\right) \tag{54}$$

where

$$\gamma = \frac{D}{H}, \quad D = EI, \quad H = \frac{4GA}{Kb^2} \tag{55}$$

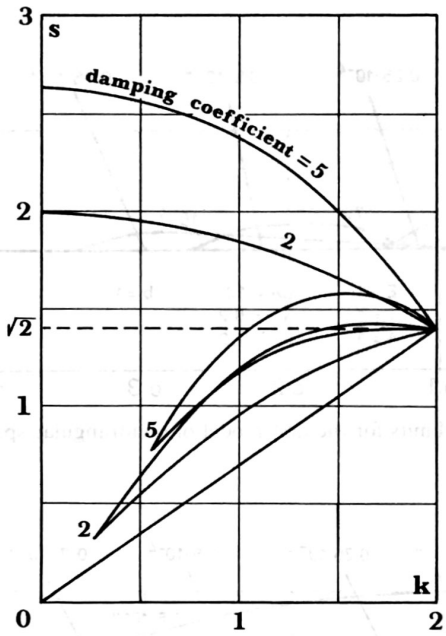

Figure 7. The influence of a damping coefficients on the stability area

EI is the flexural stiffness, G the shear modulus, A the cross-sectional area, K the shape factor for the cross section and b the length of the spatial element. The vector of nodal displacements can be determined from (53) and (54), and then unknown parameters $a, b, \ldots, h$ can be evaluated. The shape matrix can be formed. Such a procedure provides only the nodal value conformance. In stability analysis all six degrees of freedom are considered. The results are shown in Figure 8. The stability intervals are not coherent. A similar effect was observed in Figure 6 for triangular elements in axial vibrations.

We should assure the conformance of displacements on the edges of the elements. To provide the displacement continuity on edges, the shape functions described in local co-ordinates ξ, τ are introduced:

$$\mathbf{N}_i = \begin{bmatrix} (m_1 - \mu m_2)\tfrac{1}{2}(1 + \tau\tau_i) & \xi_i(m_2 - \mu m_3)\dfrac{\partial x}{\partial \xi}\dfrac{1}{2}(1 + \tau\tau_i) \\ -\dfrac{\xi_i}{\dfrac{\partial x}{\partial \xi}} m_1^{(1)}\tfrac{1}{2}(1 + \tau\tau_i) & -(m_2^{(1)} - \mu m_1^{(1)})\tfrac{1}{2}(1 + \tau\tau_i) \end{bmatrix} \quad i = 1, 2, 3, 4 \tag{56}$$

where

$$\begin{aligned} m_1 &= \tfrac{1}{4}(-\xi_0^3 + 3\xi_0 + 2) \\ m_2 &= \tfrac{1}{4}(-\xi_0^3 - \xi_0^2 + \xi_0 + 1) \\ m_3 &= \tfrac{1}{4}(-\xi_0^3 + \xi_0) \\ m_1^{(1)} &= \tfrac{3}{4}(-\xi_0^2 + 1) \\ m_2^{(1)} &= \tfrac{1}{4}(-3\xi_0^2 + 2\xi_0 + 1) \end{aligned} \tag{57}$$

$$\xi_0 = \xi\xi_i, \quad \mu = \frac{3\gamma}{1 + 3\gamma}, \quad \gamma = \frac{D}{H\left(\dfrac{\partial x}{\partial \xi}\right)^2}, \quad D = EI, \quad H = \frac{GA}{K}$$

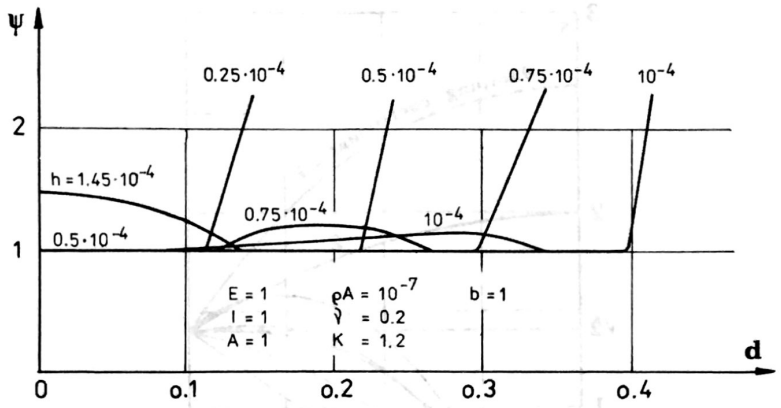

Figure 8. The stability limits for the first model of quadrangular space–time beam element

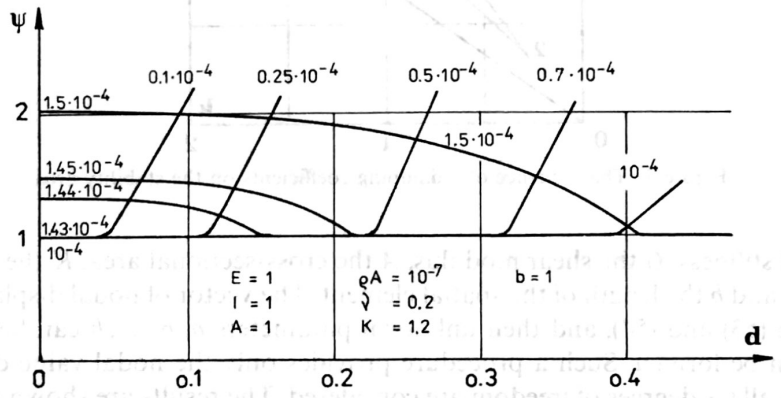

Figure 9. The stability limits for the second model of quadrangular space–time beam element

The functions of the matrix $\mathbf{N}(\xi, \tau)$ are transformed to global co-ordinates x, t by linear relations. The dependence between the shift of the inner joint d and the spectral radius ψ is depicted in Figure 9. The second model of a quadrangular element of a beam has better properties and the relation shown in Figure 9 can be expressed in terms of parameters s and ξ (Figure 10). It is seen that the extremal value of s for low values of ξ is equal to 1·5. When ξ increases the extremal s decreases and in the case when $\xi = 1$ (extremal time step)$s_{ex} = 1{\cdot}1$.

It is also interesting to verify whether the vertical (in the t-direction) shift of the joint changes the value of the spectral radius $\psi(\mathbf{T})$. To evaluate it the test problem was solved (Figure 11). The results are shown in Figure 12.

Stability of a triangular element of a beam

The conformance of displacements on edges in neighbouring elements can be provided by the assumption of a displacement distribution varying cubicly along the element sides. Evaluation of displacements, in additional six mid-side nodes, allows one to determine a polynomial of sufficiently high order over the element area. The displacements on edges are expressed in terms of nodal values by the relation

$$\begin{Bmatrix} w \\ \Theta_x \end{Bmatrix} = \mathbf{N}_1^k \boldsymbol{\delta}_i + \mathbf{N}_2^k \boldsymbol{\delta}_j = \mathbf{f}_k(\xi) \tag{58}$$

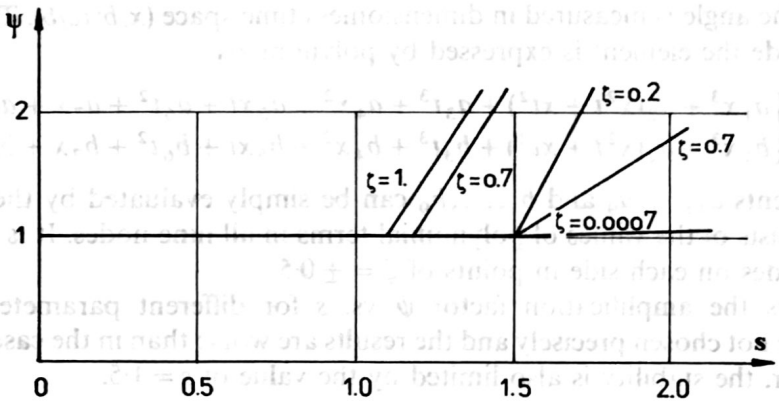

Figure 10. Stability condition for different values of ξ

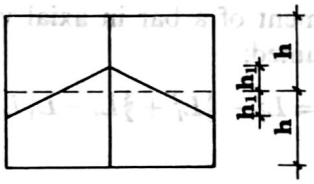

Figure 11. The scheme of the test problem

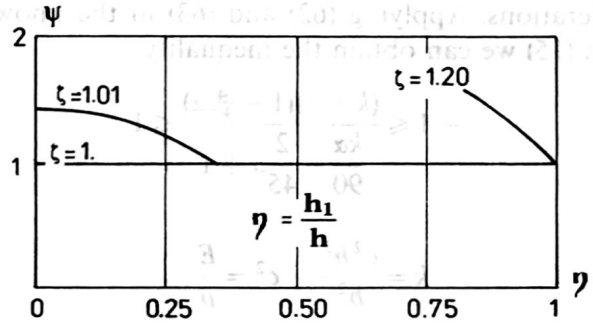

Figure 12. Amplification factor for the problem shown in Figure 11

$\boldsymbol{\delta}_i, \boldsymbol{\delta}_j$ represent the nodal displacements and $\mathbf{N}_i^k$ is the matrix of cubic and quadratic relations describing the displacements on edge k. Expression $\mathbf{N}_i^k$ are related to local co-ordinate ξ as follows:

$$\mathbf{N}_i^k(\xi) = \begin{bmatrix} N_{11i} & N_{12i} \\ N_{21i} & N_{22i} \end{bmatrix} \tag{59}$$

$$\begin{aligned} N_{11i} &= m_1 - \mu m_3 \cos^2 \alpha_k \\ N_{12i} &= \tfrac{1}{2}\xi_i l_k (m_2 - \mu m_3) \cos \alpha_k \\ N_{21i} &= -\xi_i m_1^{(1)} (1-\mu) \frac{2}{l_k} \cos \alpha_k \\ N_{22i} &= -(m_2^{(1)} - \mu m_1^{(1)}) \cos^2 \alpha_k + \tfrac{1}{2}(1 + \xi\xi_i) \sin^2 \alpha_k \end{aligned} \tag{60}$$

l_k is the length of side k of the triangle and α_k is the angle between the axis $0x$ and the edge. It must be

emphasized that the angle is measured in dimensionless time space ($x/b; tc/b$). The distribution of displacements inside the element is expressed by polynomials

$$\begin{Bmatrix} w \\ \Theta_x \end{Bmatrix} = \begin{Bmatrix} a_1x^3 + a_2(x^2t + xt^2) + a_3t^3 + a_4x^2 + a_5xt + a_6t^2 + a_7x + a_8t + a_9 \\ b_1x^3 + b_2(x^2t + xt^2) + b_3t^3 + b_4x^2 + b_5xt + b_6t^2 + b_7x + b_8t + b_9 \end{Bmatrix} \tag{61}$$

Unknown coefficients $a_1, \ldots, a_9$ and $b_1, \ldots, b_9$ can be simply evaluated by the inversion of the matrix which consists of the values of polynomial terms in all nine nodes. It is best to locate the additional two nodes on each side in points of $\xi = \pm 0{\cdot}5$.

Figure 13 shows the amplification factor ψ vs. s for different parameters ξ. The shape functions (60) were not chosen precisely and the results are worse than in the case of quadrangular elements. However, the stability is also limited by the value of $s = 1{\cdot}5$.

ATTEMPT AT AN UNCONDITIONALLY STABLE FORMULATION

We shall consider a triangular element of a bar in axial vibration. For real displacement the following shape functions were assumed:

$$N_i = L_i^3 - \tfrac{3}{2}L_i^2 + \tfrac{3}{2}L_i - L_1L_2L_3 \tag{62}$$

and for virtual displacements

$$\hat{N}_i = L_i + \alpha(-2L_i^3 + 3L_i^2 - L_i + 2L_1L_2L_3) \tag{63}$$

where L_i are the area co-ordinates, $i = 1, 2, 3$, and α is a coefficient, the evaluation of which is a subject of further considerations. Applying (62) and (63) in the known procedure (1)–(9) and considering the condition (15) we can obtain the inequality:

$$-1 \leqslant \frac{(k-1)(1-\frac{4}{45}\alpha)}{\frac{k\alpha}{90} - \frac{2}{45}\alpha + 1} \leqslant 1 \tag{64}$$

where

$$k = \frac{c^2h^2}{b^2}, \quad c^2 = \frac{E}{\rho} \tag{65}$$

In practical use α should fulfil the relation:

$$\alpha > \begin{cases} 0, & \text{for } 0 \leqslant k \leqslant 2 \\ \dfrac{30(k-2)}{3k-4}, & \text{for } k > 2 \end{cases} \tag{66}$$

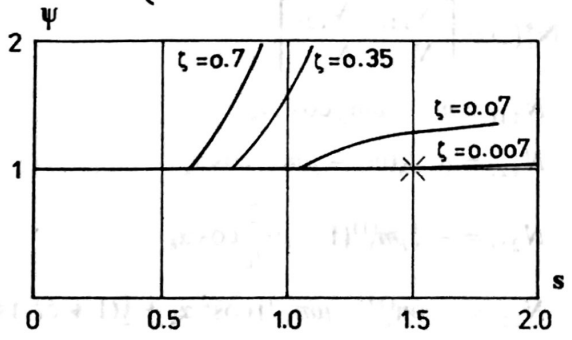

Figure 13. The stability limits for the triangular beam elements

and for the accuracy requirements should not be greater than the limit of (66). Then for any value of time step h the process (11) is stable. It seems to be important to say that the stability analysis carried out with the functions (62) and (63) for the system of elements from Figure 2(a) leads to the same stability area as in Figure 6. The value of parameter α does not affect the result. Although stiffness matrices directed by parameter α are possible for bar elements, for other types of structures analytical calculations are very complicated. All the proposals for successive elements require careful investigations.

NUMERICAL EXAMPLES AND ACCURACY DISCUSSION

To prove the correct formulation of the method and its efficiency the solutions of simple problems are presented below. Quadrangular elements of a beam were used in the vibration analysis of a cantilever. The structure was divided into three spatial elements, and one joint in the mesh was shifted in each step from the initial position (Figure 14). Results of displacements and the period of vibrations were compared with the values obtained from the computations with a rectangular mesh. Such a comparison is shown in Figure 15. Differences in results between the rectangular mesh (then the space–time finite element method can be considered as a simple time integration method) and the non-rectangular one are insignificant. For small values of ξ and for s less than 1 the relative difference of results is about 2–4 per cent. In the extreme case of $\xi \approx 1$ when the time step reaches the limitation condition and for $s = 1$ the error is much greater (even 20 per cent) but in practice such a high speed of joint deviation is rather rarely required.

The second example concerns the axial bar vibration in the case of change of its length. It is the problem with a movable edge. The length varies according to the function $l(t) = 2{\cdot}5 - 1{\cdot}5 \cos 0{\cdot}5t$. The example is somewhat similar to the problem of unreeled rope. One end is always fixed. The movement is forced by the inertia. From (35) we can find $1{\cdot}25 \leqslant \operatorname{tg}\varphi \leqslant 5{\cdot}0$. Then in Figure 6 we can see that the parameter s is limited by the inequality $s \leqslant 1{\cdot}41$ and the deviation from rectangularity $d \leqslant 0{\cdot}282$. The last condition is fulfilled in the solution. In Figure 16 the displacements in time of the free end are depicted aside the geometry changes. The first diagram describes the initial period. The second one was chosen for a later time. To eliminate the initial conditions small damping was introduced. Regularity of displacements was achieved. More detailed analysis of our results is difficult.

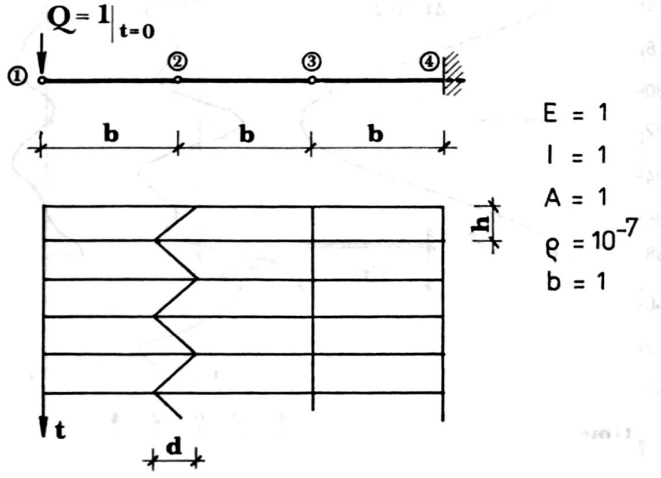

Figure 14. The approximation of the time space by the non-rectangular mesh

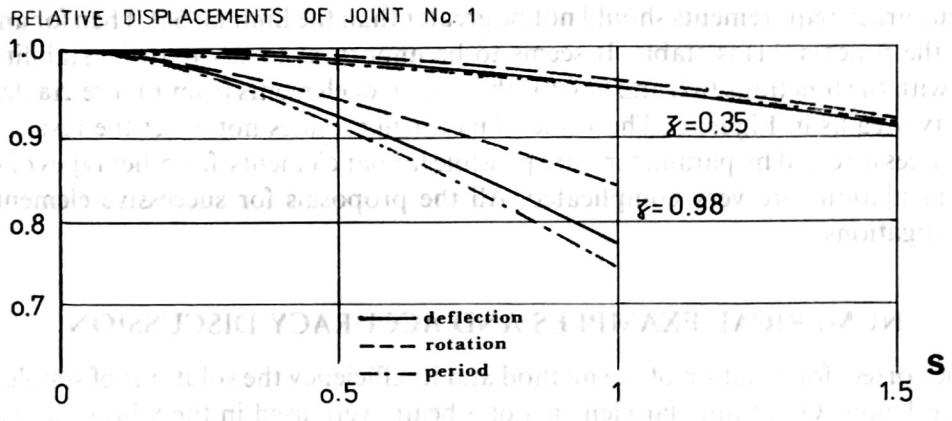

Figure 15. Results of the accuracy analysis of the quadrangular beam elements

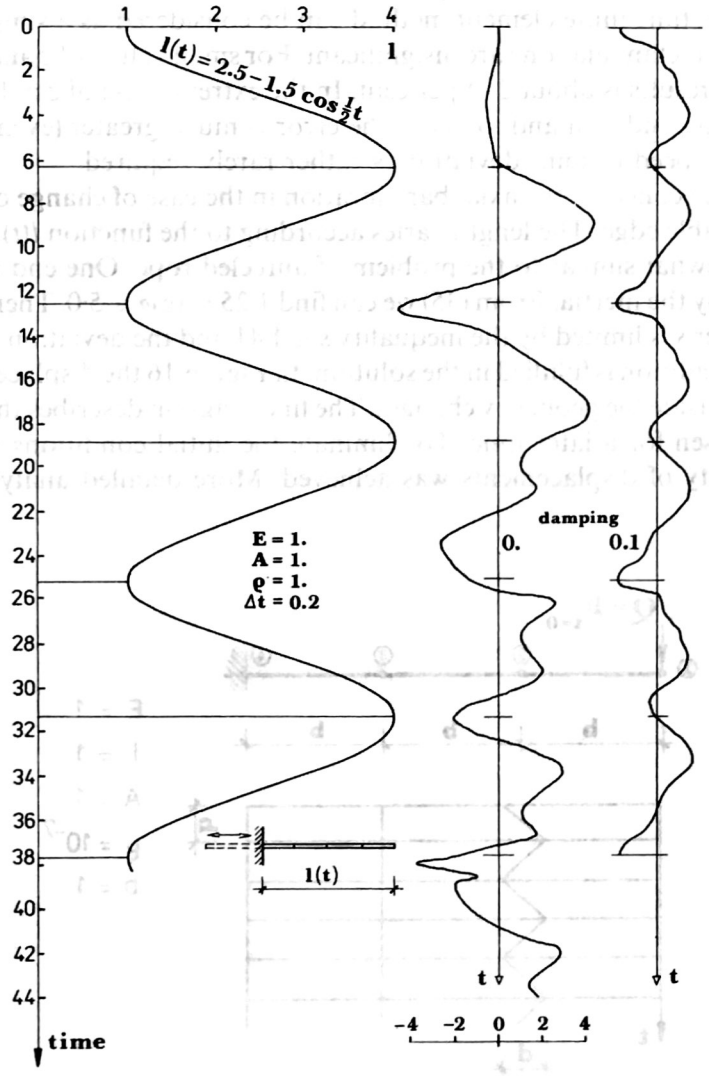

Figure 16. Displacements of the end of the bar with changeable length

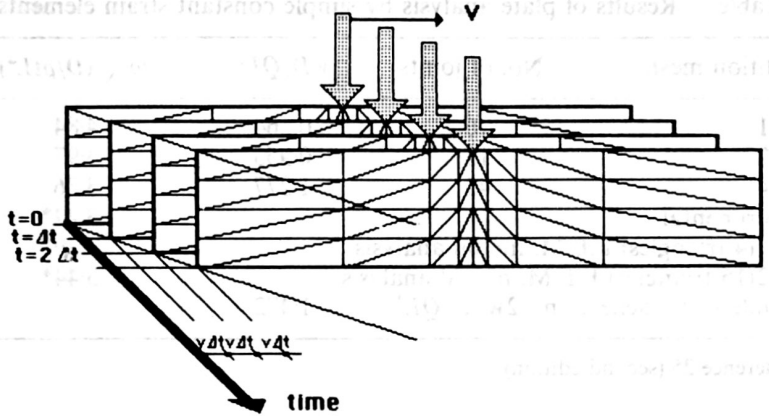

Figure 17. Movable mesh for the surface structures

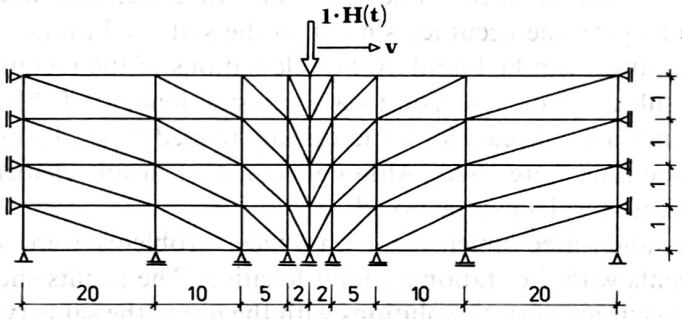

Figure 18. Spatial partition of a plate subjected in-plane by a travelling point force

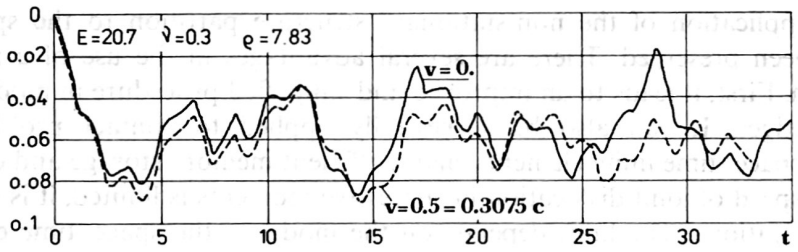

Figure 19. Displacements in time of the joint under the force

The next example shows the possibility of the use of a non-stationary partition of the structure and movable edge technique to model the infinite plane stress subjected to a moving force. In that case the division net is moved together with the force. An infinite area is bounded to the zone of significant load influence. Remaining parts are neglected. This idea is explained also in Figure 17. Such an approach allows the force to be placed all times in nodal points and to condense the partition around the subjected joint. In the experiment the mesh depicted in Figure 18 was assumed. Displacements of the subjected point in time are shown in Figure 19. Two cases were considered: for the speed of travelling force zero and non-zero. In the figure static vertical displacement is marked. The eigenvalue analysis determined the groups of basic periods of vibrations: 44·5–49·5, 19·5–21·3, 8·1–10·4 and smaller. They can be detected in the plot as reflections from the vertical rows of nodes. The static analysis gives the displacement

Table 1. Results of plate analysis by simple constant strain elements

Partition mesh	No. of joints	wD/QL^2	$\omega/\sqrt{(D/\rho tL^4)}$
2×1	6	0·564	4·84
4×2	15	0·953	3·97
8×4	45	1·277	3·36
Experimental			3.42*
2×1(4 triangles) F.E.M. modal analysis			3·39*
4×2(16 triangles) F.E.M. modal analysis			3·44*
Double static deflection	$2w_{st}D/QL^2$	1·472	

* Reference 25 (second edition)

equal to 0·09. The average displacement in dynamic analysis is about 0·06 (Figure 19). This error can be explained only by the wave propagation in the time integration process. The influence of the movable mesh is not significant and the space–time element model of plane stress in simple testing solutions gave the accuracy similar to the static solutions.

The proof of the accuracy can be found in the calculations of the rectangular cantilever plate (length:width = 2:1) subjected on one side to a Heaviside load. In Table I the amplitude and the first modal frequency are collected for a successfully refined mesh. Tetrahedral plate elements with linear shape functions were used. Although constant strain elements are used a good approach to the accurate results can be noted.

Several other two- and three-dimensional (in space) problems were solved by the use of simplex-shaped elements with the stationary joint location. The results shows that the accuracy can be related to the accuracy of static solutions with the use of the same type of shape functions.

CONCLUDING REMARKS

Conditions of application of the non-stationary structure partition to the space–time finite elements have been presented. There are several advantages in the use of a non-rectangular space–time mesh. First, it leads to an improved and simplified procedure in modelling problems with movable edges. It can also be successfully applied to contact problems. Secondly, simplex-shaped space–time finite elements enable efficient memory storage and computations.[21]

Although the speed of joint dislocation in successive moments is limited, it is sufficient in real engineering applications. The limit depends on the model of the space–time element and the type of structure. In more complex models only numerical investigations are practiced.

Modification of virtual and real shape functions allows obtaining unconditionally stable schemes considering the time step. Then the disadvantage of conditional stability can be removed.

It has been shown that within the stability region, there may exist narrow instability areas. Moreover, space–time layer partition into simplex-shaped elements should be carried out by the same space–time net (Figure 6). Changes in each step of space–time division lead to an unsymmetric stability condition (Figure 5).

REFERENCES

1. R. Bonnerot and P. Jamet, 'A second order finite element method for the one-dimensional Stefan problem', *Int. j. numer. methods eng.*, **8**, 811–820 (1974).
2. R. Bonnerot and P. Jamet, 'Numerical computation of the free boundary for the two dimensional Stefan problem by space–time finite elements', *J. Comp. Phys.*, **25**, 163–181 (1977).
3. T. Belytschko and R. Mullen, 'Stability of explicit–implicit mesh partition in time integration', *Int. j. numer. methods eng.*, **12**, 1575–1586 (1978).

4. K. S. Gupta and A. Kumar, 'Variable time step method with coordinate transformation', *Comp. Meth. Appl. Mech. Eng.*, **44,** 91–103 (1984).
5. C. I. Bajer, 'Non-stationary division by the space–time finite element method in vibration analysis', in M. Petyt and H. F. Wolfe (eds), *Proc. Second Int. Conf. on Recent Advances in Structural Dynamics*, ISVR Southampton, 1984, pp. 161–170.
6. J. T. Oden, 'A general theory of finite elements, I. Topological considerations, II. Applications', *Int. j. numer. methods eng.*, **1,** 205–221, 247–259 (1969).
7. J. H. Argyris and D. W. Sharpf, 'Finite element in space and time', *Nucl. Eng. Des.*, **10,** 456–469 (1969).
8. I. Fried, 'Finite element analysis of time-dependent phenomena', *AIAA J.*, **7,** 1170–1173 (1969).
9. Z. Kaczkowski, 'The method of finite space–time elements in dynamics of structures', *J. Tech. Phys.*, **16,** 69–84 (1975).
10. Z. Kaczkowski, 'General formulation of the stiffness matrix for the space–time elements', *Archiwum Inzynierii Ladowej*, **25,** 351–357 (1979).
11. Z. Kaczkowski and J. Langer, 'Synthesis of the space–time finite element method', *Archiwum Inzynierii Ladowej*, **26,** 11–17 (1980).
12. R. Riff and M. Baruch, 'Time finite element discretization of Hamilton's law of varying action', *AIAA J.*, **22,** 1310–1318 (1984).
13. Z. Kacprzyk and T. Lewinski, 'Comparison of some numerical integration methods for the equations of motion of systems with a finite number of degrees of freedom', *Eng. Trans.*, **31,** 213–240 (1983).
14. K. C. Park, 'Practical aspects of numerical time integration', *Comp. Struct.*, **7,** 343–353 (1977).
15. R. Mullen and T. Belytschko, 'An analysis of an unconditionally stable explicit method', *Comp. Struct.*, **16,** 691–696 (1983).
16. T. R. J. Hughes, 'Stability, convergence and growth and decay of energy of the average acceleration method in nonlinear structural dynamics', *Comp. Struct.*, **6,** 313–324 (1976).
17. W. K. Liu, T. Belytschko and Y. F. Zhang, 'Implementation and accuracy of mixed-time implicit–explicit methods for structural dynamics', *Comp. Struct.*, **19,** 521–530 (1984).
18. T. J. R. Hughes and T. E. Tezduyar, 'Stability and accuracy analysis of some fully-discrete algorithms for the one dimensional second order wave equation', *Comp. Struct.*, **19,** 665–668 (1984).
19. R. Riff and M. Baruch, 'Stability of time finite elements', *AIAA J.*, **22,** 1171–1172 (1984).
20. R. Jeltsch, 'Stability and accuracy of different schemes for hyperbolic problems', *J. Comp. Appl. Math.*, **12–13,** 91–108 (1985).
21. C. I. Bajer, 'Triangular and tetrahedral space–time finite elements in vibration analysis', *Int. j. numer. methods eng.*, **23,** 2031–2048 (1986).
22. C. I. Bajer, 'Microcomputer applications of non-rectangular space–time finite elements in vibration analysis—direct joint-by-joint procedure', in R. A. Adey (ed.), *Engineering Software IV, Proc. 4th Int. Conf.*, Springer-Verlag, Berlin, 1985, pp. 7–3 to 7–16.
23. K. Bathe and E. Wilson, *Numerical Methods in Finite Element Analysis*, Prentice-Hall, Englewood Cliffs, New Jersey, 1976.
24. J. Legras, *Methods et Techniques de l'Analyse Numerique*, Dunod, Paris, 1971.
25. O. C. Zienkiewicz, *The Finite Element Method*, 2nd edn, McGraw-Hill, London, 1977.